Check for updates

Origin analysis of paleo-overpressure in source rocks based on logging response characteristics: a case study of the Chang 7 member in the Triassic Yanchang formation, Longdong area, Ordos Basin, China

Kaitong Xu[1]*, Yujia Huang[2], Minggang Tang[1], Jiahao Wu[3] and Tengfei Ma[4]

[1]PetroChina Tarim Oilfield Company, Exploration Department, Korla, China, [2]Korla Branch of Research Institute of Bureau of Geophysical Prospecting INC, China National Petroleum Corporation, Korla, China, [3]PetroChina Tarim Oilfield Company, Kela Oil and Gas Production Management Zone, Korla, China, [4]PipeChina Group, Chongqing, China

The identification of the origins of source rock palaeo-overpressure based on logging response parameters is frequently influenced by the presence of organic matter. To accurately identify the paleo-overpressure origin of source rocks and employ an appropriate method for paleo-pressure calculation, this study proposes a quantitative approach to assess the influence of organic matter content on overpressure analysis. The findings demonstrate that the presence of organic matter in Chang 7 shale leads to an increase in acoustic time difference and a decrease in density. After incorporating the multi-component rock equivalent volume model correction, it is evident that the paleo-overpressure observed in the Chang 7 member is not attributed to undercompaction but rather to fluid expansion mechanisms. In conjunction with the acoustic velocity-density palte method, the paleo-overpressure of the Chang 7 member is attributed to undercompaction and expansion resulting from hydrocarbon generation. The pressure evolution of the Chang 7 member has been reconstructed based on the identification of its paleo-overpressure origin. The distribution characteristics of paleo-pressure recovered based on hydrocarbon generation expansion exhibit a strong correlation with the reservoir. The reliability of the correction method for organic matter influence is demonstrated. The proposed method is not only applicable for the investigation of paleo-pressure, but also holds significant implications for the assessment of pressure within organic-rich intervals.

KEYWORDS

origin identification of palaeo-overpressure, logging response, correction of organic matter content, Chang 7 member, Ordos Basin

1 Introduction

Overpressure is a prevalent geological phenomenon in petroleum basins, posing persistent challenges to researchers in the field of petroleum geology regarding its genesis and spatial distribution. (Hunt, 1990; Fu, et al., 2000; Chen and Wang, 2001; Zha, et al., 2002; Mohsin, et al., 2023). The initial research on formation pressure primarily caters to engineering requirements in ensuring the safety of drilling operations. The analysis of overpressure has emerged as a pivotal focus in the investigation of oil and gas reservoir formation, as our comprehension of this phenomenon continues to deepen. (Cao, et al., 2006). Historically, the focus of oil and gas exploration endeavors has predominantly revolved around the prevailing distribution characteristics of formation pressure. The proposal and successful application of various quantitative models for overpressure calculation have been witnessed across multiple disciplines. (Zhang, et al., 2013; Fan, et al., 2015; Su, et al., 2019; Qiu, et al., 2020a; Shabani, et al., 2022; Shabani, et al., 2023; Su, et al., 2023; Tang, et al., 2023). However, it appears that the paleo-pressure characteristics during the period of hydrocarbon accumulation exert a more pronounced influence on the distribution of hydrocarbons. It is crucial to develop a quantitative model for the recovery of paleo-overpressure. Currently, the predominant models utilized for reconstructing paleo-overpressure are predominantly forward models that necessitate a comprehensive understanding of the origins of overpressure (Zhao, et al., 2017; Nazemi, et al., 2021). The conventional approaches for identifying the origins of overpressure are based on the atypical response exhibited by various logging parameters within the interval of overpressure. The logging parameters, however, exhibit strong multi-solution due to various factors such as rock composition, fluid properties, and borehole diameter expansion. (Meyer and Nederlof, 1984; Zhang et al., 2002). The identification of overpressure origins can be significantly influenced in dark mudstones with hydrocarbon generation potential, particularly due to the low density and velocity of organic matter (Chen, 1996).

The Chang 7 member of the Yanchang Formation constitutes the primary source rock interval for the Triassic in the Ordos Basin, characterized by a suite of semi-deep or deep lacustrine facies dark mud shale (Guo and Li, 2016). Although the current formation pressure of the Chang 7 member is equal to or less than the hydrostatic pressure at the corresponding depth (Wang, 2012; Zhang, 2017), anomalies in log data such as velocity and density indicate a high likelihood of paleo-overpressure. Many scholars posited that the paleo-overpressure of the Chang 7 member is attributed to imbalanced compaction, as evidenced by significant anomalies in logging data. However, the author considered this case to be a prototypical example illustrating how the composition of organic matter can influence the identification outcomes of overpressure origins.

This paper presented a quantitative approach to assess the impact of organic matter content on overpressure analysis. Using Chang 7 Member as a case study, the pressure evolution process is reconstructed by identifying the origins of paleo-overpressure. The distribution characteristics of paleo-pressure recovered through origin analysis exhibit a strong correlation with the oil reservoirs. This confirms the robustness of the correction method in accounting for organic matter effects. This method is not only applicable for paleo-pressure analysis, but also holds significant implications for pressure assessment of organic-rich formations.

2 Geological background

The Ordos Basin is located in the central part of mainland China and the west of North China Platform. It is the second largest sedimentary basin in China. It was once a constituent of the Great North China Basin during the Paleozoic era, and subsequently transformed into a depression basin in the late Mesozoic period, exhibiting typical craton sedimentary basin characteristics. The basin margin deformation exhibits a high degree of intensity, while the main part of the basin displays a relatively simple structure. The regional structure of the basin is characterized by a gentle and broad monocline dipping towards the west. According to the fundamental geological conditions of the basin, including gravity, magnetic and electric characteristics, basement burial depth and current structure, as well as tectonic evolution, the basin can be classified into six second-order structural units: Yimeng uplift, Weibei uplift, Jinxi flexural fold belt, Yishan slope, Tianhuan depression and western margin thrust belt (Figure 1).

The Chang 7 member studied in this paper was deposited during the maximum lacustrine transgression, resulting in a vast water body with interbedded dark mudstones and oil shales of shallow-deep lacustrine facies (Yang, et al., 2017). The study area is situated in the southwestern part of the basin, the Chang 7 member and the Chang 8 Member formed a high-quality source rock-reservoir combination (Yao, et al., 2014) (Figure 1). As a significant source rock segment, the current formation pressure of Chang 7 Member in this area is predominantly normal or negative (Yao, et al., 2013). However, the significant amount of oil and gas present in the shallower formation indicates that the Chang 7 member possesses high excess pressure, which serves as a driving force for oil and gas migration. Additionally, the presence of acoustic time differences and density anomalies in Chang 7 provides further evidence for the existence of paleo-overpressure.

3 Background of methods for analyzing the origins of overpressure

The primary origins of overpressure that receive significant attention in the field include disequilibrium compaction, hydrocarbon-generating expansion, conduction, chemical compaction, and tectonic action (Dickinson, 1953; Hubbert and Rubey, 1959; Barker, 1972; Magara, 1975; Law and Dickinson, 1985; Freed and Peacor, 1989; Swarbrick and Osborne, 1998; Yardley and Swarbrick, 2000). The origins of overpressure are directly related to the choice of a palaeo-pressure recovery model, and therefore a method for identifying the origins has been continuously explored and summarised. In general, abnormal pressure segments are often accompanied by regular abnormal changes in logging curves. Hermanrud et al. noted that the overpressure section causes significant anomalies in logging data closely related to porosity,
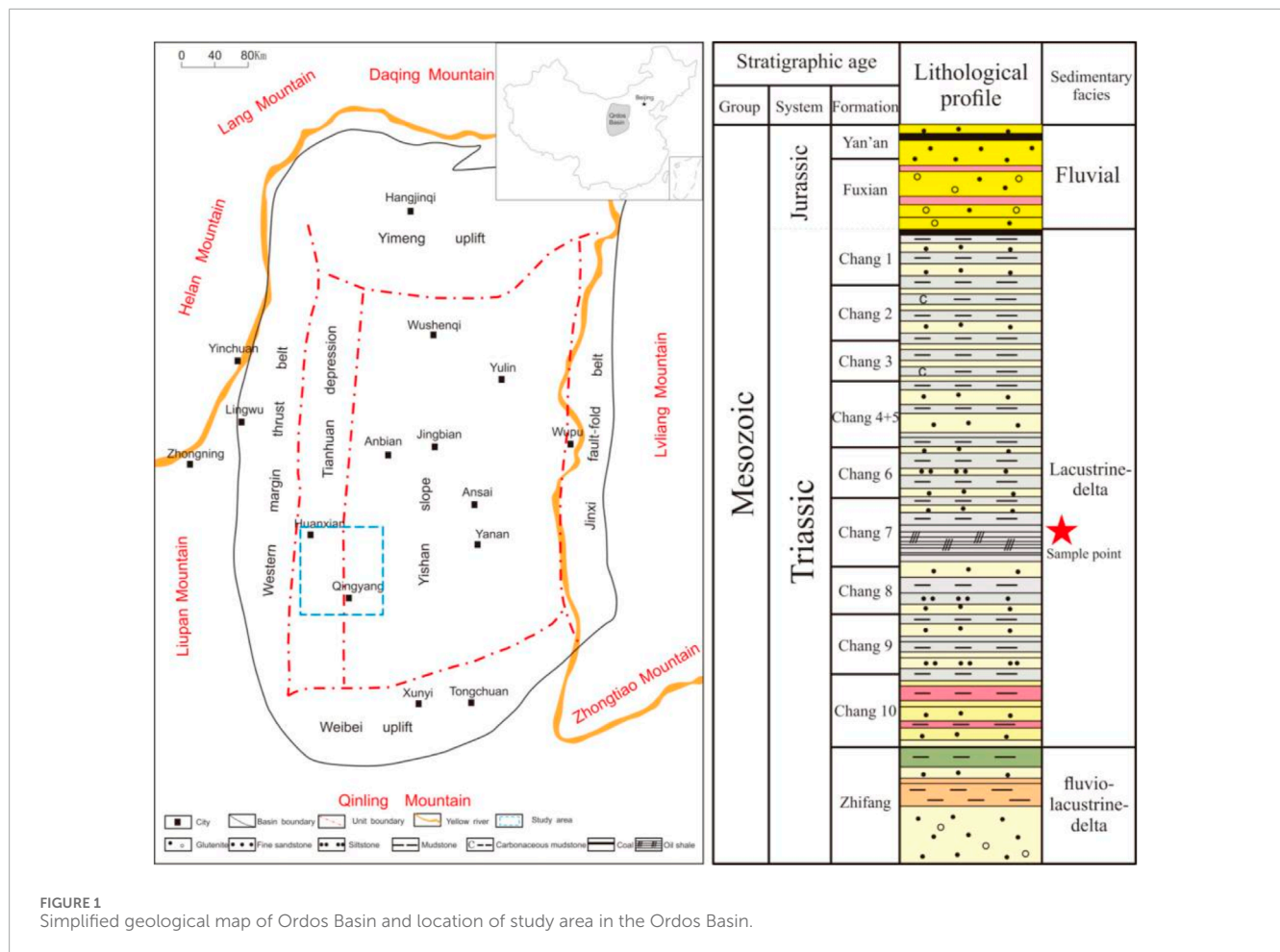
FIGURE 1
Simplified geological map of Ordos Basin and location of study area in the Ordos Basin.

such as acoustic time difference, density, resistivity and neutrons (Hermanrud, et al., 1998). Although he noted the abnormal response of some geophysical parameters to overpressure, he did not distinguish the origins of overpressure.

When studying the response characteristics of abnormal high-pressure logging in the Not formation in Haltenbanken area, Bowers divided the logging data into volume properties (density, neutron) and conductivity properties (acoustic time difference, resistivity) according to the different sensitivities of density, acoustic time difference, neutron and resistivity (Bowers, 2002). He emphasized that the overpressure formed when the compaction stops or slows down, such as disequilibrium compaction, often alters both volumetric and conductivity properties. The overpressure formed under the internal pressure of fluid expansion often has little effect on the volume properties, but it changes the structural characteristics of the pores and causes obvious anomalies in the conductivity properties. The pressure generated by fluid expansion can obviously change the throat in the pore throat structure, and with the increase of expansion pressure, the width of the throat becomes larger, and the number of throat decreases, which will lead to the increase of resistance and the decrease of acoustic velocity.

3.1 Log combination contrast method

Comparing the anomaly amplitudes of different logging parameters can often pose challenges due to their varying physical interpretations To address this problem, Bowers in 2002 summarized log data maps to distinguish between disequilibrium compaction and fluid expansion (Bowers, 2002). As depicted in Figure 2, the overpressure resulting from disequilibrium compaction causes an inversion of resistivity, acoustic velocity, and density. In the process of burial, once the geological body located at point A is sealed and undergoes disequilibrium compaction, it will eventually reach state C. For this kind of disequilibrium compaction, obviously the same electrical properties and similar lithology correspond to the same vertical effective stress, which is also the basic principle of the equilibrium depth method to predict formation pressure. Therefore, a simple method for identifying the origin of overpressure is obtained, that is, the resistivity, acoustic time difference and density at the same depth are read in the reverse section, while extending vertically up to the normal trend line. If the intersection point of the extension line of the log data and the normal trend line is basically at the same depth, then the
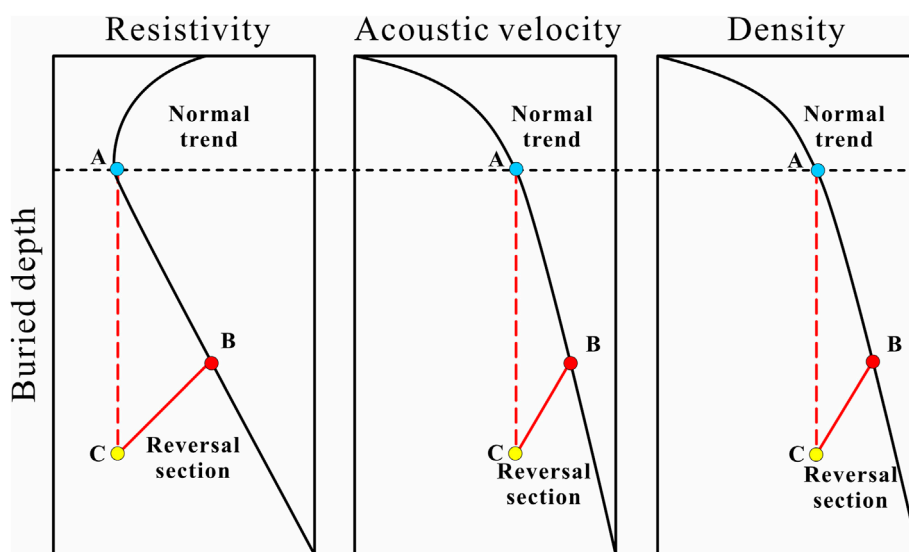
FIGURE 2
Response characteristics of disequilibrium compaction overpressure logging (Bowers, 2002).

overpressure at the reverse section is caused by disequilibrium compaction.

Generally, elastic rebound does not occur under disequilibrium compaction. However, the overpressure caused by the fluid expansion tends to show elastic rebound. The occurrence of the rebound phenomenon often exerts a significant influence on individual logging data. The rebound of volume property is much smaller than that of conduction property. Thus, the resistivity, acoustic velocity, and density at the same depth are read in the reverse section, while extending vertically up to the normal trend line. If the resistivity and velocity extensions intersect with the normal trend line at basically the same depth, but the density extensions intersect with the normal trend line at a deeper depth than the other two data, then the overpressure at the inversion section is caused by fluid expansion (Figure 3).

3.2 Calculated porosity contrast method

Similarly, in order to compare the overpressure response of different physical parameters, Tingay simultaneously converted the acoustic time difference and density data into the corresponding porosity for comparative analysis (Tingay, et al., 2007). The amplitude of porosity anomaly, calculated based on volume and conduction properties, remains consistent in the overpressure section resulting from disequilibrium compaction. In the overpressure segment of fluid expansion, the anomaly amplitude of porosity calculated by volume properties is relatively low or almost no anomalies. This normalization method avoids subjective influence and is simple to operate, which has been recognized by many scholars.

This paper mainly compares the calculated results of porosity with density and acoustic time difference as the main parameters,

and the calculation formula is as follows:

$$\Phi_{den} = \frac{\rho_{ma} - \rho_b}{\rho_{ma} - \rho_f} \tag{3.1}$$

(Tingay, et al., 2007)where, Φ_{den} is density porosity, decimal; ρ_{ma} is the skeleton density of mudstone, g/cm^3; ρ_f is pore fluid density, g/cm^3; ρ_b is the value point density, read by the density log, g/cm^3

$$\Phi_{sonic} = \frac{1}{C_p} \frac{\Delta t - \Delta t_{ma}}{\Delta t_f - \Delta t_{ma}} \tag{3.2}$$

(Raymer, et al., 1980)where, Φ_{sonic} is acoustic porosity; Δt_{ma} is the acoustic time difference of shale skeleton, and the empirical value is 223.39 μs/m; Δt_f is the pore fluid acoustic time difference,625 μs/m; Δt is the measured acoustic time difference of the value point,μs/m; C_p is the compaction coefficient of shale, and the empirical value is taken.

3.3 Velocity-density crossplot method

In addition to the above two methods, there is a more direct method, that is, to choose the velocity and density to compare, and draw the acoustic velocity - density crossplot plate (O'Connor and Lahann, 2011; Tingay and Morley, 2013; Dasgupta, et al., 2016) (Figure 4). During the loading process, the speed and density exhibit synchronous variations along the loading curve. Since disequilibrium compaction is only a pause in the compaction process, the speed and density still fall on the loading curve. Because the velocity variation is much greater than the density in the overpressure section caused by unloading, most of the data points fall under the loading curve.
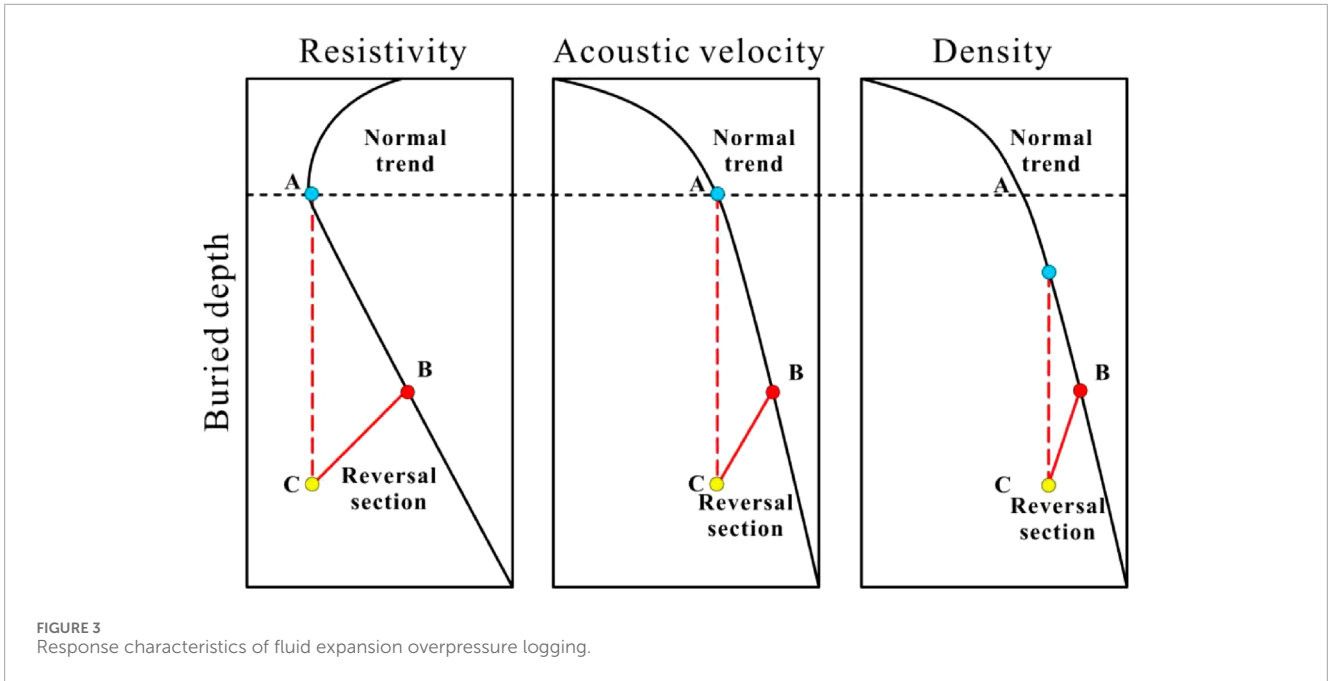
FIGURE 3
Response characteristics of fluid expansion overpressure logging.
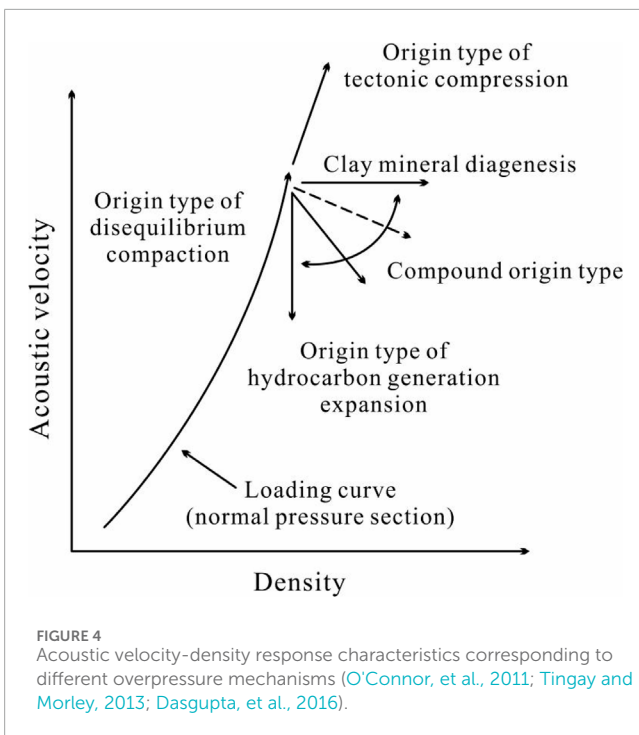

FIGURE 4
Acoustic velocity-density response characteristics corresponding to different overpressure mechanisms (O'Connor, et al., 2011; Tingay and Morley, 2013; Dasgupta, et al., 2016).

4 Materials and methods

4.1 Quantitative method for correction of organic matter content

In this paper, using unit volume as correction unit, the source rock is divided into four parts: rock skeleton, organic matter, hydrocarbon and formation water, and the non-source rock is divided into rock skeleton, hydrocarbon and formation water. By introducing organic matter into the multi-component equivalent volume model, the increment of acoustic time difference and density loss caused by organic matter in Chang 7 shale can be obtained. Ultimately, the acoustic time difference and density logging curves can be derived by eliminating the influence of organic matter.

The multi-component equivalent volume correction model of source rock is as follows (Li, et al., 2021):

$$\Delta t_s = \Delta t_{ma} v_{ma} + \Delta t_{om} v_{om} + \Delta t_H v_H + \Delta t_w v_w \quad (3.3)$$

$$\rho = \frac{m_{ma} + m_{om} + m_H + m_w}{V_{ma} + V_{om} + V_H + V_w} = \rho_{ma} v_{ma} + \rho_{om} v_{om} + \rho_H v_H + \rho_w v_w \quad (3.4)$$

$$v_{ma} + v_{om} + v_H + v_w = 1 \quad (3.5)$$

$$v_H + v_w = \varphi \quad (3.6)$$

$$v_H = S_H \cdot \varphi \quad (3.7)$$

where, Δt_s is the acoustic time difference of source rock obtained from logging data; Δt_{ma} is the acoustic time difference of shale skeleton, taken as a constant 223.39 μs/m; Δt_{om} is the acoustic time difference of organic carbon, and the theoretical value is 550 μs/m; Δt_H is the acoustic time difference of hydrocarbon (oil and gas), taken as a constant 780 μs/m; Δt_w is the acoustic time difference of formation water, taken as a constant 625 μs/m (Li, et al., 2016; Yang, et al., 2018); v_{ma}, v_{om}, v_H and v_w are the volume of shale skeleton, organic matter, hydrocarbons and formation water as a percentage of the total volume, respectively; φ is the porosity of the source rock of Chang 7 member, a decimal number, which is 1.55% after investigation (Liang, et al., 2020); S_H is the oil saturation, a decimal number, and the median value is 0.58 based on the shale oil data of the reference well (Wu, et al., 2016). ρ is the source rock density obtained from logging data; ρ_H is the density
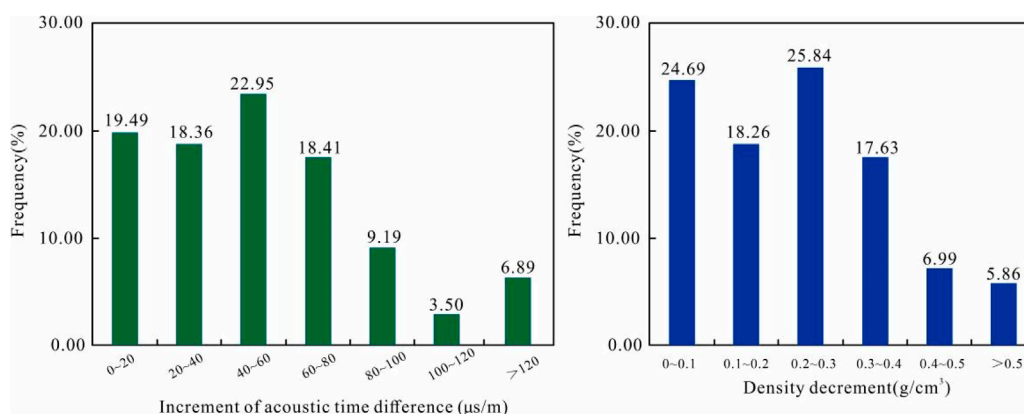
FIGURE 5
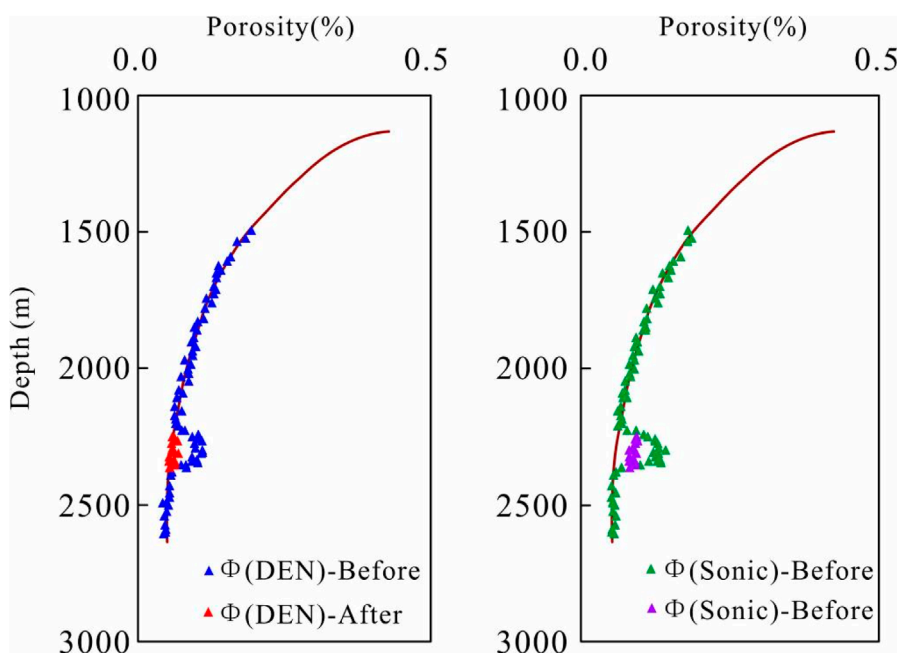Quantitative effects of organic matter in Chang 7 on density and acoustic time difference.

FIGURE 6
Difference in acoustic time difference porosity-density porosity before and after correction for organic matter.

of hydrocarbons, taken as a constant 0.8 g/cm³; ρ_w is the formation water density, taken as a constant 1.05 g/cm³; ρ_{ma} is the skeleton density of shale, taken as a constant 2.68 g/cm³; ρ_{om} is the organic carbon density, the theoretical value is 1.1 g/cm³; m_{ma}, m_{om}, m_H and m_w are the mass of shale skeleton, organic carbon, hydrocarbon and formation water, respectively; V_{ma}, V_{om}, V_H and V_w are the volumes of shale skeleton, organic matter, hydrocarbons and formation water, respectively.

When the organic matter content of Chang 7 is quantitatively evaluated, the result is the mass percentage of organic carbon, but the volume percentage needs to be used in the correction. The mass percentage of TOC can be converted to the volume percentage of TOC according to the conversion coefficient of organic matter mass

volume (Tang and Sun, 2019), that is:

$$v_{om} = \frac{V_{om}}{V_{rock}} = \frac{\rho_{rock}}{\rho_{om}} \omega_{TOC} = \frac{\rho_{ma}}{\rho_{om}} k \omega_{TOC} \qquad (3.8)$$

where, ω_{TOC} is the percentage of organic carbon mass, decimal; ρ_{rock} is the rock density obtained from logging data; ρ_{ma} is the skeleton density of shale, taken as a constant 2.68 g/cm³; ρ_{om} is the organic carbon density, taken as the theoretical value; k is the conversion coefficient of organic carbon, which is related to the type and maturity of organic matter (Yang, et al., 2018; Xu, et al., 2019). since the organic matter type of mud shale in Chang 7 member in the study area is mainly type I, the experience value of 1.25 is taken,
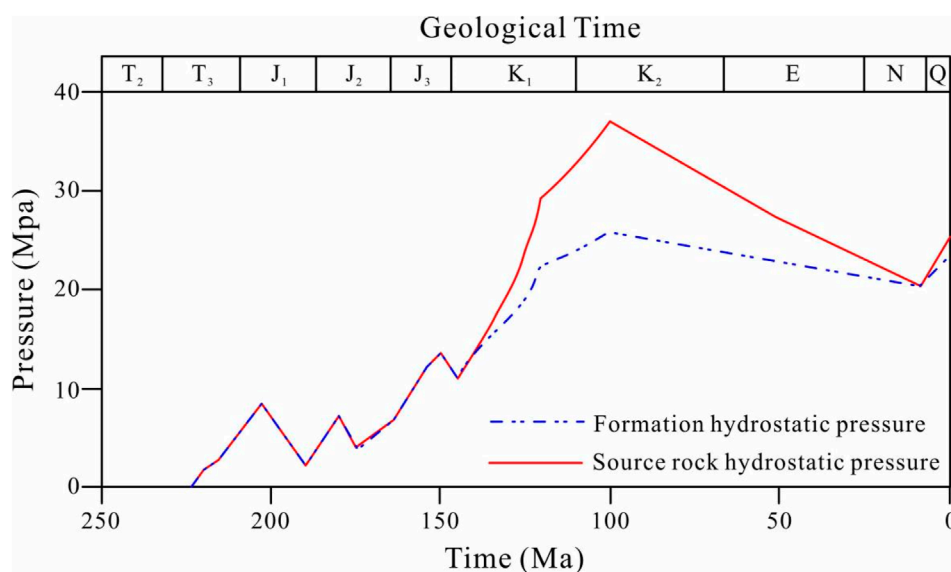
FIGURE 7
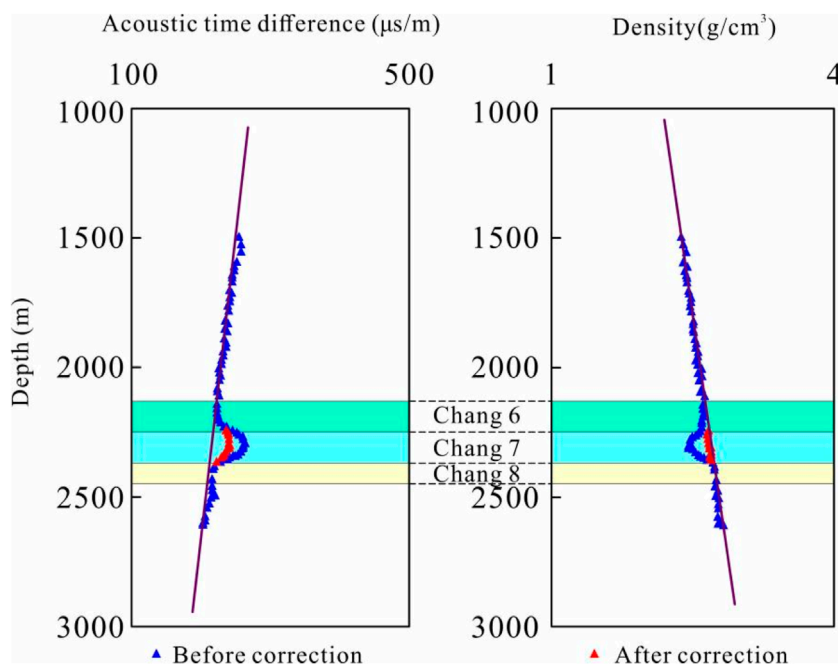Diagram of formation pressure evolution process of source rock in Chang 7 member.

FIGURE 8
Log response characteristics before and after correction.

and the above formula is transformed into:

$$v_{om} = 3.045\omega_{TOC} \tag{3.9}$$

The rock components in non-source rocks can be considered as the framework of the rock and the fluid filling its pores. Since the shale of Chang 7 non-hydrocarbon source rock does not have the ability to generate hydrocarbon, and the shale is relatively dense, the oil and gas outside the shale pores can rarely be injected into the

shale, so the hydrocarbon content in the pore fluid can be ignored. The physical volume model of non-source rock only includes rock skeleton and formation water, which can be expressed as:

$$\Delta t'_s = \Delta t_{ma}v_{ma} + \Delta t_w v_w = (1-\phi)\Delta t_{ma} + \phi\Delta t_w \tag{3.10}$$

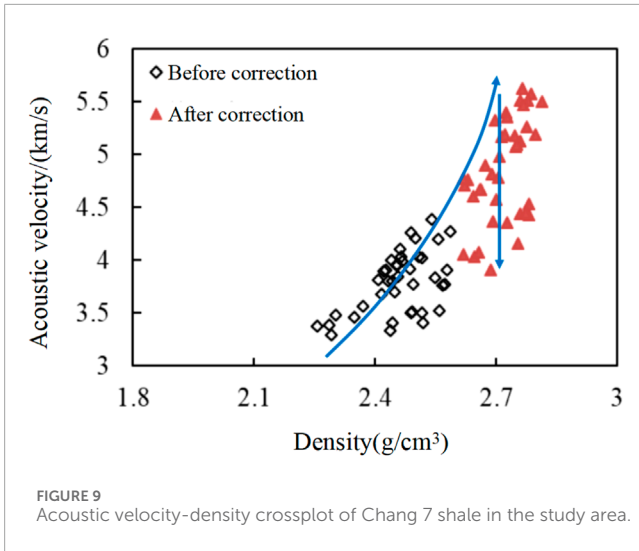$$\rho' = \frac{m_{ma} + m_w}{V_{ma} + V_w} = (1-\phi)\rho_{ma} + \phi\rho_w \tag{3.11}$$

where, $\Delta t'_s$ and ρ' are the acoustic time difference and density of non-source rock respectively, and ϕ is the porosity of non-source rock shale. The porosity calculated based on the acoustic time difference data shows that the average porosity of non-source rock in Chang 7 member of the study area is 0.92%.

The increase of acoustic time difference and decrease of acoustic density caused by organic matter are as follows:

$$\Delta t_{TOC} = \Delta t_s - \Delta t'_s = \Delta t_{ma}(\phi - \varphi - v_{om}) + \Delta t_{om} v_{om} + \Delta t_H S_H \varphi$$
$$+ \Delta t_w [\varphi(1 - S_H) - \phi] \tag{3.12}$$

$$\rho_{TOC} = \rho - \rho' = \rho_{ma}(\phi - \varphi - v_{om}) + \rho_{om} v_{om} + \rho_H S_H \varphi$$
$$+ \rho_w [\varphi(1 - S_H) - \phi] \tag{3.13}$$

4.2 Methods of calculating palaeo-pressure

4.2.1 For disequilibrium compaction

The current predominant approach for quantifying overpressure induced by disequilibrium compaction is the equilibrium depth method. This method is based on the absolute correspondence between porosity and effective stress, so it can be combined with the buried history recovered by PetroMod2014 basin simulation system to calculate the pressure. The specific calculation steps are as follows: 1) Record the burial depth of the formation at the beginning of the rapid sedimentation and the effective stress at the depth under normal pressure; 2) Record the buried depth of the formation at the end of rapid sedimentation and lithostatic pressure at this depth; 3) The difference value is taken as the pore pressure at the end of sedimentation, and the excess pressure caused by disequilibrium compaction is calculated further combined with the hydrostatic pressure at this depth.

4.2.2 For hydrocarbon-generating expansion

This time, the calculation model of hydrocarbon generation pressurization established by Guo Xiaowen according to the

conservation of space and matter is adopted (Guo, 2010), and its formula is as follows:

$$\Delta P = \frac{AFM_k[\alpha D(1 - P_h C_o) - 1]}{C_w V_{wl} \rho_k + (1 - AF)C_k M_k + \alpha AFM_k DC_o}$$

where, ΔP is the excess pressure generated by hydrocarbons, MPa; M_k is the mass of kerogen, calculated from the original TOC, $M_k = \rho r \times TOC$, ρr is 2.6 g/cm^3; P_h is the hydrostatic pressure, $P_h = \rho wgh$, h is the burial depth during the accumulation period, ρw is the groundwater density (1.05×10^3 kg/m^3), g is 9.8 m/s^2; C_w is the compression coefficient of water, 0.44×10^{-3} MPa^{-1} (Amyx, et al., 2020); C_k is the compression coefficient of kerogen, 1.4×10^{-3} MPa^{-1} (DuBow, 1984), C_0 is the compression coefficient of petroleum, 1.0×10^{-3} MPa^{-1} (obtained from high pressure physical property data); $D = \rho_k / \rho_0$, ρk is 1.2 g/cm^3, ρ_0 is the measured underground crude oil density, 863.6 kg/m^3; V_{w1} is the volume of pore water, $\varphi_1 = V_{w1}$, φ_1 is the porosity during reservoir accumulation, which is read by Petromod software; A=HI/1000, is the original hydrogen index; F is the conversion rate of kerogen, which is read by PetroMod software; α is the oil residual coefficient.

5 Results

5.1 The influence of organic matter

It is calculated that the increment of acoustic time difference caused by organic matter in Chang 7 shale is between 2.56 and 169.78 µs/m, mainly distributed in the range of 2.56–80 µs/m. The density decrement caused by organic matter ranges from 0.01 to 0.61 g/cm^3, and the main distribution ranges from 0.01 to 0.4 g/cm^3 (Figure 5).

5.2 Identification results of the origin of paleo-overpressure

Figure 6 shows the difference between density porosity and acoustic time difference of Chang 7 member before and after correction. Both kinds of porosity before correction deviate significantly from the normal trend of porosity change, and the difference between density porosity and acoustic time difference of porosity is small. The paleo-overpressure of Chang 7 member is caused by disequilibrium compaction. After correction, the density porosity reverts to the normal trend line, and the porosity undergoes compaction in accordance with standard procedures. Although the deviation degree of acoustic time difference porosity decreased, it still deviated from the normal trend, and the difference between density porosity and acoustic time difference porosity varied from little to obvious, indicating that the paleo-overpressure of Chang 7 member was not caused by undercompaction, but by fluid expansion mechanism.

5.3 Paleo-pressure recovery results

Based on the revised velocity and density response characteristics, the primary cause of paleo-overpressure formation
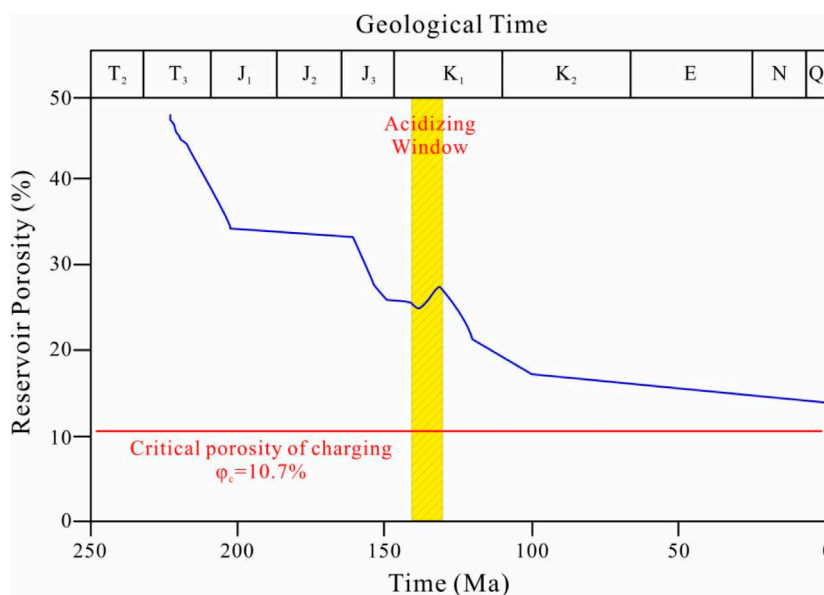
FIGURE 10
Evolution diagram of sandstone porosity in Chang 8 member (Modified by Wang, et al., 2016).
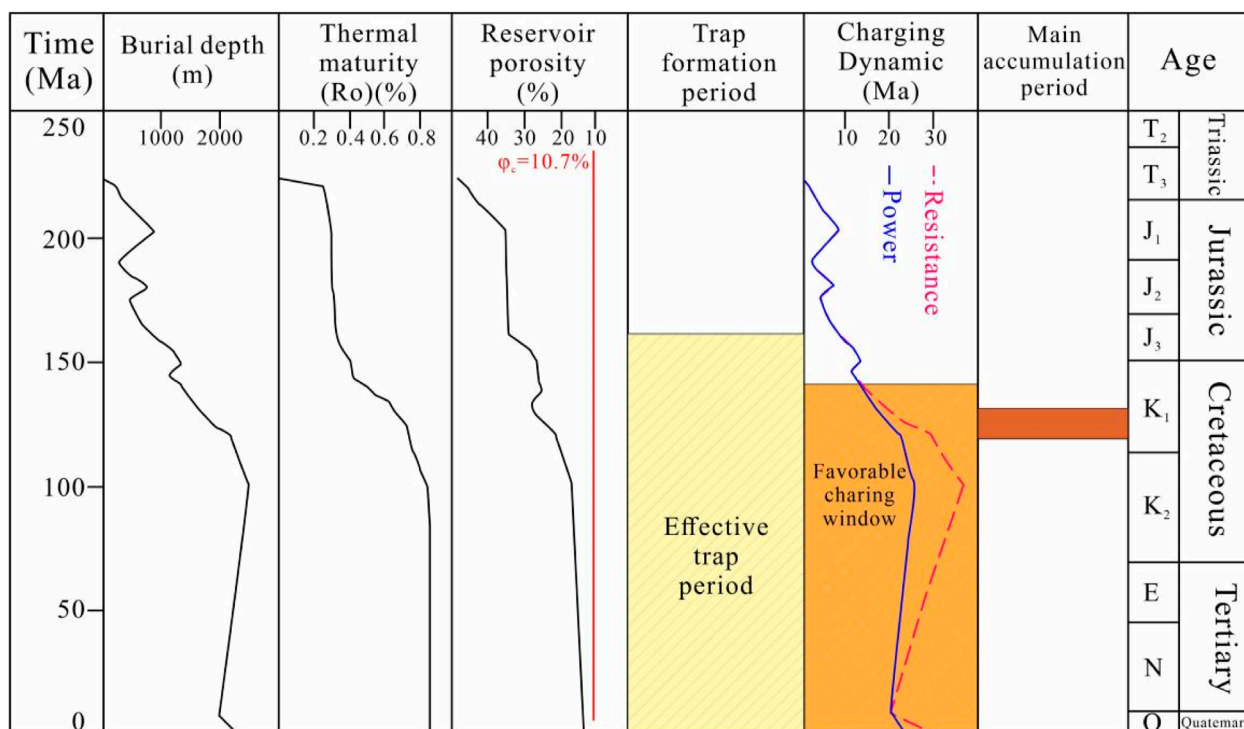
FIGURE 11
Comprehensive map of reservoir formation factors evolution.

in the study area is attributed to fluid expansion resulting from hydrocarbon generation within Chang 7 Member source rock. The hydrocarbon generation pressurization recovery model was employed to analyze the paleo-pressure recovery results of a reservoir in the study area, as illustrated in Figure 7. The hydrostatic pressure data comes from Li (Li and Guo, 2011). It can be seen

FIGURE 12
Contour map of pressure coefficient of Chang-7 during oil accumulation period and its relationship with oil reservoirs.

a right deflection anomaly increase; while the density also deviates from the normal compaction trend line and reverses, showing a left deflection anomaly increase. After correction, the acoustic time difference still deviates from the normal compaction trend line as the depth of burial increases, but shows a characteristic decrease in leftward deflection; while the density basically returns to the normal compaction trend line or its vicinity, without deflection (Figure 8).

The acoustic velocity-density response characteristics of shale in the study area are shown in Figure 9, and the acoustic velocity-density crossplot before and after correction also presents different changing trends. Before correction, the subpoint of Chang 7 member segment fall on the loading curve of disequilibrium compaction and are distributed on or near the loading curve, indicating that the paleo-overpressure of Chang 7 member segment is caused by disequilibrium compaction. After correction, part of the paleo-overpressure is still located near the loading curve, but most of it is located near the hydrocarbon generation expansion trend line, indicating that the paleo-overpressure of Chang 7 member is not only caused by undercompaction, but also caused by the hydrocarbon generation expansion of mature organic matter. In short, after correction, the acoustic velocity is higher than that before correction, the density does not change significantly, and the acoustic velocity gradually decreases, which accords with the characteristics of hydrocarbon generation expansion. Through the method of acoustic velocity-density plate, it is found that the paleo-overpressure of Chang 7 member is caused by two compound origins: undercompaction and hydrocarbon generation expansion.

that the source rocks of Chang 7 Member began to generate hydrocarbon in the early Cretaceous and reached the peak of hydrocarbon generation until 100 Ma ago. Simultaneously, the formation pressure gradually accumulated during the process of hydrocarbon generation. The maximum excess pressure is 10–15 MPa. During the period of 100 Ma~2 Ma, with the continuous uplift of the strata, the hydrocarbon generation stopped, and the formation pressure also continued to lose, and finally formed the present distribution characteristics dominated by normal pressure.

6 Discussion

6.1 The correction model can eliminate the influence of organic matter and determine the correct origin of paleo-overpressure

After correction of the multi-component rock equivalent volume correction model, the effect of high organic content on the acoustic time difference and density in the Chang 7 section was excluded, and the characteristics of the Chang 7 section logging curve were significantly different before and after correction. Before correction, as the burial depth increases, the acoustic time difference does not fit the normal compaction trend line and reverses, showing

6.2 It is difficult for the paleo-pressure caused by undercompaction to break through the resistance

According to the results of porosity simulation and recovery (Wang, et al., 2016) (Figure 10), although porosity evolved slowly between 200 Ma and 160 Ma, burial depth did not increase to a large extent during the same period. Therefore, the overpressure calculated based on the unbalanced compaction model will be smaller. Furthermore, numerous uplift events occurred during this period, posing challenges in preserving the accumulated excess pressure for subsequent oil and gas migration.

Through the comprehensive simulation of the evolution process of various hydrocarbon accumulation factors (Chen, et al., 2018), the time of hydrocarbon generation and pressurization is well matched with other factors. At the same time, the overpressure caused by hydrocarbon generation can reach up to 30MPa, while the highest charging resistance of the reservoir is less than 20 MPa. During the 140 Ma~2 Ma period, the long-term stable sourced-reservoir pressure difference promotes the formation of a large favorable charging window (Figure 11). It is proved that the paleooverpressure is caused by hydrocarbon generation, and the supercharging of hydrocarbon generation is one of the important factors affecting the hydrocarbon accumulation in the target layer in the study area.

6.3 The high structure with overpressure is a favorable area for reservoir distribution

The distribution characteristics of paleo-pressure in the mudstone of Chang 7 member have been determined by extrapolating the results of hydrocarbon generation pressurization model to the entire area. c. The pressure distribution is controlled by the sedimentary facies zone, and the more developed the mudstone, the greater the pressure, which is just opposite to the present trend. The mudstone formation experienced a general development of overpressure during the accumulation period, with a gradual decrease in overpressure amplitude from east to west. The reservoir is located in the transition area from high pressure to low pressure (Figure 12).

Based on the study on the fluid pressure characteristics of the Chang 7 mudstone formation, it is found that the fluid pressure characteristics of the present mudstone are obviously adjusted compared with the accumulation period, which is related to the regional tectonic inversion, geothermal decline and the evolution of overlying pressure. The oil reservoirs are primarily distributed in the transitional zone of mudstone pressure gradients during the accumulation period. The abnormal high pressure in mudstone is the main driving force of hydrocarbon migration and accumulation.

7 Conclusion

Paleo-overpressure is common in Chang-7 source rocks in the study area, and the content of organic matter will cause obvious deviation in logging response characteristics, which will affect the correct identification of the origin of paleo-overpressure.

The multi-component rock equivalent volume correction model can eliminate the influence of organic matter and determine the correct origin of paleo-overpressure. It is found that the origin of hydrocarbon generation expansion paleo-overpressure is dominant in the study area, and the correction model is effective.

The distribution characteristics of paleo-pressure recovered based on the analysis of hydrocarbon generation expansion have a good relationship with the reservoir, and the reservoir is mainly distributed in the high structure where the overpressure is relatively developed.

Data availability statement

The original contributions presented in the study are included in the article/Supplementary material, further inquiries can be directed to the corresponding author.

Author contributions

KX: Writing–original draft, Writing–review and editing. YH: Conceptualization, Data curation, Formal Analysis, Writing–original draft. MT: Funding acquisition, Investigation, Methodology, Writing–original draft. JW: Project administration, Resources, Software, Writing–review and editing. TM: Supervision, Writing–review and editing.

Conflict of interest

Authors KX, MT, and JW were employed by PetroChina Tarim Oilfield Company. Author YH was employed by China National Petroleum Corporation. Author TM was employed by PipeChina Group.

Publisher's note

All claims expressed in this article are solely those of the authors and do not necessarily represent those of their affiliated organizations, or those of the publisher, the editors and the reviewers. Any product that may be evaluated in this article, or claim that may be made by its manufacturer, is not guaranteed or endorsed by the publisher.

References

Amyx, J. W., Bass, D. M., and Whiting, R. L. (1960). Petroleum reservoir engineering: physical properties. https://lmsspada.kemdikbud.go.id/pluginfile.php/679010/mod_resource/content/1/Amyx%2-%20Petroleum%20Reservoir%20Engineering_compressed.pdf.

Barker, C. (1972). Aquathermal pressuring-role of temperature in development of abnormal-pressure zones. *AAPG Bull.* 56, 2068–2071. doi:10.1306/819A41B0-16C5-11D7-8645000102C1865D

Bowers, G. L. (2002). Detecting high overpressure. *Lead. edge* 21, 174–177. doi:10.1190/1.1452608

Cao, H., Gong, J. J., and Wang, G. F. (2006). The cause of overpressure and its relationship with reservoir forming. *Nat. Gas. Geosci.* 03, 422–425. doi:10.1007/s10552-013-0268-z

Chen, B. N., and Wang, N. (2001). Research advance and method practice of anomalous fluid pressure. *Pet. Geol. Recovery Effic.* 01, 35–37+3.

Chen, H. H., Zhu, X. M., Chen, C. F., Yin, W., and Shi, R. S. (2018). The coupling relationship of reservoir densification history and hydrocarbon emplacement

in tight sandstone reservoir: a case study of the Chang8 oil member, Yanchang Formation, southern Ordos Basin. *Acta Sedimentol. Sin.* 36, 401–414. doi:10.7623/syxb201803001

Chen, Y. C. (1996). Using the logging data to study and evaluate the source rocks. *Geophys. Prospect. Petroleum* 01, 99–106.

Dasgupta, S., Chatterjee, R., and Mohanty, S. P. (2016). Magnitude, mechanisms, and prediction of abnormal pore pressure using well data in the Krishna–Godavari Basin, east coast of India. *AAPG Bull.* 100, 1833–1855. doi:10.1306/05131615170

Dickinson, G. (1953). Geological aspects of abnormal reservoir pressures in Gulf Coast Louisiana. *AAPG Bull.* 37, 410–432. doi:10.1306/5ceadc6b-16bb-11d7-8645000102c1865d

DuBow, J. (1984). "Temperature effects," in *Mechanics of oilshale [A]: london.* Editors K. P. Chong, and J. W. Smith (Amsterdam, Netherlands: Elsevier Applied Science Publishers), 523–577.

Fan, C. Y., Wang, Z. L., Wang, A. G., Zhang, X., Zhang, Y. S., and Kong, H. X. (2015). Mechanisms for overpressure generation and origin of overpressured gas anaaquifer

layers, Eboliang structure belt, northernQaidam Basin. *Acta Pet. Sin.* 36, 699–706+714. doi:10.7623/syxb201506006

Freed, R. L., and Peacor, D. R. (1989). Geopressured shale and sealing effect of smectite to illite transition. *AAPG Bull.* 73, 1223–1232. doi:10.1306/44b4aa0a-170a-11d7-8645000102c1865d

Fu, G., Lv, Y. F., Xue, Y. C., and Yang, M. (2000). Evolution characteristics of pressure sealing of mudstone caprock and its research significance. *Acta Pet. Sin.* 03, 41–44+109. doi:10.7623/syxb200003008

Guo, X. W. (2010). *Overpressure evolution caused by hydrocarbon generation in petroliferous basins-two cases studies from dongying and baiyun depressions.* Wuhan, China: China University of Geosciences.

Guo, Y. Q., and Li, W. H. (2016). *Tight reservoir characteristics and reservoir enrichment rule of triassic Yanchang Formation in Ordos Basin.* Beijing, China: Petroleum Industry Press.

Hermanrud, C., Wensaas, L., and Teige, G. M. (1998). *Shale porosities from well logs on haltenbanken (offshore mid-Norway) show No influence of overpressuring.* Australia: GeoScience.

Hubbert, M. K., and Rubey, W. W. (1959). Role of fluid pressure in mechanics of overthrust faultingi. mechanics of fluid-filled porous solids and its application to overthrust faulting. *GSA Bull.* 70, 115–166. doi:10.1130/0016-7606(1997)109<0643:CBQBFT>2.3.CO;2

Hunt, J. M. (1990). Generation and migration of petroleum from abnormally pressured fluid compartments. *AAPG Bull.* 74, 1–12. doi:10.1306/0c9b21eb-1710-11d7-8645000102c1865d

Law, B. E., and Dickinson, W. W. (1985). Conceptual model of origin of abnormally pressured gas accumulations in low permeability reservoirs. *AAPG Bull.* 69, 1295–1304. doi:10.1306/AD462BD7-16F7-11D7-8645000102C1865D

Li, C., Zhang, L. G., Luo, X. R., Zhang, L. Q., Hu, C. Z., Yang, P., et al. (2016). A quantitative method for revising abnormally high sonic data in rich-organic rock during compaction study. *J. China Univ. Pet. Ed. Nat. Sci.* 40, 77–87. doi:10.3969/j.issn.1673-5005.2016.03.010

Li, J., Zhao, J. Z., Hou, Z. Q., Zhang, S. P., and Chen, M. N. (2021). Origins of overpressure in the central Xihu depression of the East China Sea shelf basin. *AAPG Bull.* 105, 1627–1659. doi:10.1306/02262118112

Li, X. W., and Guo, X. W. (2011). *Study on the characteristic of hydrocarbon accumulation mesozoic formation in zhenjing block,Ordos Basin.* Chengdu, China: Chengdu University of Technology.

Liang, X. W., Guan, Z. X., Niu, X. B., Guan, P., Dan, W. D., Feng, S. B., et al. (2020). Reservoir characteristics of shale oil in Chang 7 member of Yanchang Formation Ordos Basin. *Nat. Gas. Geosci.* 31, 1489–1500.

Magara, K. (1975). Importance of aquathermal pressuring effect in Gulf coast. *AAPG Bull.* 59, 2037–2045. doi:10.1306/83d921db-16c7-11d7-8645000102c1865d

Meyer, B. L., and Nederlof, M. H. (1984). Identification of source rocks on wireline logs by density/resistivity and sonic transit time/resistivity crossplots. *AAPG Bull.* 68, 121–129. doi:10.1306/ad4609e0-16f7-11d7-8645000102c1865d

Mohsin, M., Tavakoli, V., and Jamalian, A. (2023). The effects of heterogeneity on pressure derived porosity changes in carbonate reservoirs, Mishrif formation in SE Iraq. *Petroleum Sci. Technol.* 41, 898–915. doi:10.1080/10916466.2022.2070210

Nazemi, M., Tavakoli, V., Rahimpour-Bonab, H., and Sharifi-Yazdi, M. (2021). Integrating petrophysical attributes with saturation data in a geological framework, Permian-Triassic reservoirs of the central Persian Gulf. *J. Afr. Earth Sci.* 179, 104203. doi:10.1016/j.jafrearsci.2021.104203

O'Connor, S., and Lahann, R. S. (2011). Geologically-driven pore fluid pressure models and their implications for petroleum exploration. Introduction to thematic set. *Geofluids* 11, 1468–8123. doi:10.1111/j.1468-8123.2011.00354.x

Qiu, N., Liu, Y., Liu, W., and Jia, J. (2020a). Quantitative reconstruction of formation paleo-pressure in sedimentary basins and case studies. *Sci. China Earth Sci.* 63, 808–821. doi:10.1007/s11430-019-9556-8

Qiu, N., Liu, Y., Liu, W., and Jia, J. (2020b). Quantitative reconstruction of formation paleo-pressure in sedimentary basins and case studies. *Sci. China Earth Sci.* 63, 808–821. doi:10.1007/s11430-019-9556-8

Raymer, L. L., Hunt, E. R., and Gardner, J. S. (1980). "An improved sonic transit time-to-porosity transform," in SPWLA Annual Logging Symposium. SPWLA, Lafayette, Louisiana, July, 1980.

Shabani, F., Amini, A., Tavakoli, V., Chehrazi, A., and Gong, C. (2023). 3D basin and petroleum system modelling of the early cretaceous play in the NW Persian Gulf. *Geoenergy Sci. Eng.* 226, 211768. doi:10.1016/j.geoen.2023.211768

Shabani, F., Amini, A., Tavakoli, V., Honarmand, J., and Gong, C. (2022). 3D forward stratigraphic modeling of the Albian succession in a part of the northeastern margin of the Arabian Plate and its implications for exploration of subtle traps. *Mar. Petroleum Geol.* 145, 105880. doi:10.1016/j.marpetgeo.2022.105880

Su, A., Chen, H., Feng, Y. X., Zhao, J. X., Lei, M., and Nguyen, A. D. (2023). Distal accumulation of leaked gas from deep overpressured zone: the case of the Yanan Sag, Qiongdongnan Basin, South China Sea. *Mar. Petroleum Geol.* 151, 106181–181. doi:10.1016/j.marpetgeo.2023.106181

Su, A., Chen, H., Lei, M., Li, Q., and Wang, C. (2019). Paleo-pressure evolution and its origin in the pinghu slope belt of the xihu depression, east China sea basin. *Mar. Petroleum Geol.* 107, 198–213. doi:10.1016/j.marpetgeo.2019.05.017

Swarbrick, R. E., and Osborne, M. J. (1998). A review of mechanics for generation overpressure insedimentary basin. *AAPG Mem.* 70, 13–34.

Tang, T. Z., and Sun, L. D. (2019). *Petroleum geophysical logging.* Beijing: Petroleum Industry Press.

Tang, Y., Wu, Y., Wang, R., Huang, Y., Xue, Y., Chen, Z., et al. (2023). Fluid evolution and paleo-pressure recovery by Raman quantitative analysis in the Shahejie Formation of the western slope belt in Dongpu Sag, Bohai Bay Basin, China. *Front. Earth Sci.* 10, 1059–1909. doi:10.3389/feart.2022.1059909

Tingay, M. R. P., Hillis, R. R., Swarbrick, R. E., Morley, C. K., and Damit, A. R. (2007). 'Vertically transferred'overpressures in Brunei: evidence for a new mechanism for the formation of high-magnitude overpressure. *Geology* 35, 1023–1026. doi:10.1130/g23906a.1

Tingay, M. R. P., Morley, C. K., Laird, A., Limpornpipat, O., Krisadasima, K., Pabchanda, S., et al. (2013). Evidence for overpressure generation by kerogen-to-gas maturation in the northern Malay Basin. *AAPG Bull.* 97, 639–672. doi:10.1306/09041212032

Wang, Y. (2012). *Research on the relationship between abnormal pressureand hydrocarbon accumulation of lower YanchangFormation in the central and western erdos basin.* Kirkland, Washington: Northwest University.

Wang, Y., Li, S. T., Mou, W. W., and Yan, C. C. (2016). Tight reservoir characteristics and porosity evolution of Chang8-1 in western Jiyuan area. *Lithol. Reserv.* 28, 59–66.

Wu, Y., Hou, Y. T., Li, H. G., and Xian, C. G. (2016). Application of high-precision formation elements logging to shale oil ReservoilEvaluationA case study of seventh member of Yanchang Formation, Ordos Basin. *Unconv. Oil Gas* 3, 1–10.

Xu, Z. Y., Zhao, J. Z., and Li, J. (2019). The impact of organic matter content on overpressure analysis and itscorrection method in the first member of Cretaceous Qingshankou Formation,Placanticline area, Songliao Basin. *Oil Gas. Geol. (Beijing, China)* 40, 938–946.

Yang, D. Q., Liu, B., Jia, M. C., Liu, T. X., Jin, L., and Wang, H. L. (2018). Misunderstandings of high organic matter abundance mudstone compaction and quantitative correction methods. *Fault-Block Oil Gas. Field* 25, 29–33.

Yang, H., Liang, X. W., Niu, X. B., Feng, S. B., and You, Y. (2017). Geological conditions for continental tight oil formation and the main controllingfactors for the enrichment: a case of Chang 7 Member, Triassic Yanchang Formation.Ordos Basin, NW China. *Pet. Explor. Dev.* 44, 11–19. doi:10.1016/s1876-3804(17)30003-4

Yao, T. L., Deng, X. Q., Zhao, Y. D., Han, T. Y., Chu, M. J., and Pang, J. L. (2013). Characteristics of tight oil in triassic Yanchang Formation,Ordos Basin. *Pet. Explor. Dev.* 40, 161–169. doi:10.1016/s1876-3804(13)60019-1

Yao, T. L., Duan, Y., Xu, L., Luo, A. X., Deng, X. Q., Zhao, Y. D., et al. (2014). Pressure evolution and oil-gas migration and accumulation in mesozoic palaeo-strata in longdong area of the Ordos Basin. *Nat. Gas. Geosci.* 25, 649–656.

Yardley, G. S., and Swarbrick, R. E. (2000). Lateral transfer: a source of additional overpressure? *Mar. Petroleum Geol.* 17, 523–537. doi:10.1016/s0264-8172(00)00007-6

Zha, M., Qu, J. X., and Zhang, W. H. (2002). The relationship between overpressure and reservoir forming mechanism. *Pet. Explor. Dev.* 01, 19–23. doi:10.0000/1000-0747-29-165

Zhang, F. Q., Wang, Z. L., Wu, Y. S., Yang, J. H., and Luo, X. R. (2002). A method for eliminating geology factors of affecting compaction trendline: an example from yinggehai basin. *Acta Sedimentol. Sin.* 02, 326–332.

Zhang, F. Q., Wang, Z. L., Zhong, H. L., Yang, C., and Wang, J. T. (2013). Recognition model and contribution evaluation of main overpressure FormationMechanisms in sedimentary basins. *Nat. Gas. Geosci.* 24, 1151–1158. doi:10.9774/GLEAF.978-1-909493-38-4_2

Zhang, H. Y. (2017). *Overpressure by Hydrocarbon Generation as the dynamic for tight oil migration-A case of Yanchang tight oil from Ordos Basin.* Chengdu, China: Southwest Petroleum University.

Zhao, J. Z., Li, J., and Xu, Z. Y. (2017). Advances in the origin of overpressures in sedimentary basins. *Acta Pet. Sin.* 38, 973–998. doi:10.7623/syxb201709001